Optimization of pulsed-wave Doppler ultrasound for estimation of influx/efflux in oil and gas boreholes while drilling using conventional LWD transducers

Shivanandan Indimath [a,*], Stefano Fiorentini [a], Bjarne Rosvoll Bøklepp [b], Jørgen Avdal [a], Svein-Erik Måsøy [a]

[a] Center for Innovative Ultrasound Solutions (CIUS), Department of Circulation and Medical Imaging, Norwegian University of Science and Technology, Trondheim, 7491, Norway
[b] 3TDI EDT EDP Data Management Architecture and Analytics, Equinor ASA, Trondheim, 7053, Norway

ARTICLE INFO

ABSTRACT

The extraction of oil and gas typically involves drilling boreholes through various subsurface strata. Abrupt variations in the formation properties can severely compromise the borehole stability if the drilling process is not adequately controlled. Certain events can result in influx/efflux of fluids through fissures or fractures in the borehole wall. This causes a destabilization in the drilling operation known as a "kick" which, if not controlled, may lead to serious well incidents. Modern drilling operations are continuously monitored using various logging-while-drilling (LWD) tools including ultrasonic imaging to assure a high degree of control over the drilling process. However, none of these tools directly monitor fluid flow from influx/efflux events in the borehole while drilling. This work explores the use of pulsed-wave (PW) Doppler ultrasound for mapping fluid influx through fractures in the borehole wall using ultrasonic transducers similar to those used in conventional LWD tools. This paper aims to define optimal parameters for PW Doppler specific to its application in LWD. The use of short pulse-lengths (2–4 wavelengths) for velocity estimation is explored. Mean velocity estimates with a standard deviation of 0.05 m/s is demonstrated using pulse-length of 4 wavelengths and the lower limit on radial flow velocities estimates was found to be around 0.2 m/s (15 ml/s from ⌀10 mm orifice) for LWD conditions. Furthermore, imaging the fracture geometry with a high SNR of about 30 dB is demonstrated using the power of PW Doppler spectra and compared with conventional pulse-echo amplitude imaging used in LWD tools. Estimation of lateral dimensions of the fracture using the power of PW Doppler spectra with a resolution approaching the size of the point-spread function of the probe has also been demonstrated.

1. Introduction

Drilling of boreholes is a standard practice for the recovery of oil and gas from subsurface reservoirs. The depth of these boreholes can be several kilometers below sea level and there may be many variations in the formation properties through various subsurface strata along the depth of the borehole. In addition to the naturally occurring formation fractures, the drilling process inherently induces cracks and fissures along the borehole wall and under normal conditions this does not pose any problems for the drilling operations. However when the stresses induced by drilling are too high, the fissures may open up and cause an unwanted influx/efflux of formation/drilling fluids between the formation and borehole (Brudy and Zoback, 1999). Such conditions are one of the main causes for a phenomenon known as "kick", that occur due to sudden loss of stability in the pressure of the fluid column in the borehole. In severe cases where these kick events cannot be controlled, a loss of the wellbore may occur, sometimes also accompanied with a loss of the drill-string due to collapse of the wellbore, resulting in severe economic liability for the operators. Thus the drilling operations are carefully monitored using various logging-while-drilling (LWD) tools and post drilling well logging techniques (Ellis and Singer, 2007). However, to the best of the authors' knowledge there is no LWD technique currently in use to measure or monitor such influx/efflux event.

Commonly used early kick detection systems monitor various operational parameters from the drilling platform (Nayeem et al., 2016). These systems amongst other tools usually also involve the monitoring
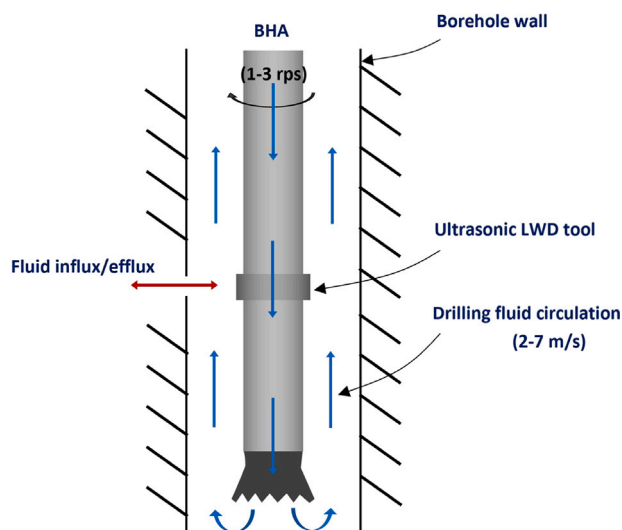
Fig. 1. Schematic of a BHA with an ultrasonic LWD tool inside a borehole indicating the flow of drilling mud and fluid influx/efflux.

of drilling fluid volume and pressure being circulated into the drill-string (Orban et al., 1991). In the event of a kick that may occur several kilometers down the borehole, it takes several minutes before the effects of a kick are measurable in the operational parameters by these systems. Such information delay, in critical cases, may lead to blowouts.

There has been a consistent effort to develop LWD tools for monitoring fluid influx/efflux in boreholes. Some of these techniques include physical measurement of the pressure of the drilling fluid near the drill bit (Andrew, 1942; Grosso and Jr., 1988), use of radioisotopes for measuring changes in density of drilling fluid (Murphy and Coope, 1985), measurement of dielectric constant of the drilling fluid (Rodney, 1990) and acoustic techniques measuring the sound speed in drilling fluid (Wu, 2008) or the amount of gas bubbles in the drilling fluid (Taherian and Garcia-Osuna, 2016). Most of these tools however are either not very sensitive to small influx/efflux or require additional instrumentation to be added to the bottom hole assembly (BHA) which is neither very practical nor economical in an already complex drilling system.

The use of ultrasonic measurements in LWD is common for imaging the borehole surface for fissures, borehole profile and assessment of rheological properties of the formation (Ellis and Singer, 2007). Fig. 1 is a schematic representation of a typical BHA with ultrasonic LWD tools. The drilling fluid is circulated from the surface, through the center of the drill-string, through the drill bit nozzles into the borehole, carrying the rock cuttings back to the surface through the annulus between the borehole and the BHA. The typical flow velocity of the drilling fluid along this axial component is around 2–7 m/s (Ferguson and Klotz, 1954). While drilling, the typical rotation speed of the BHA is about 1–3 revolutions-per-second (rps) (Chevron et al., 2021). In the event of an influx/efflux, the formation/drilling fluid will flow along the radial direction as depicted in Fig. 1. It is desirable that the same ultrasonic LWD tools can also be used for the detection and quantification of influx/efflux in the boreholes while drilling as it would eliminate the need for major modifications or increased complexity in the BHA.

Considerable work has been done by various researchers to evaluate Doppler ultrasound for characterizing radial flow in boreholes. Pulsed wave (PW) and continuous wave (CW) Doppler ultrasound methods for estimating radial flow volumes and blockages during production logging are described by Razi et al. (1995), Ravenscroft et al. (1998) and Nyhavn et al. (1999). Although radial flow quantification in production logging may seem similar to influx/efflux while drilling, the

speed of rotation of the tool and frequency of ultrasonic probes used in LWD make the direct application of production logging tools to LWD quite challenging. PW Doppler ultrasound has been studied further under laboratory conditions for post-drilling well logging by Saito and Niitsuma (2001) and Monnier and Guillermin (2003). These papers however have not investigated the applicability of the their methods under LWD conditions. Details of the Doppler ultrasound parameters used, signal processing methods and their influence on the radial flow estimates have also not been discussed in these papers.

This paper evaluates the performance of PW Doppler ultrasound for the quantification of radial flow velocity from small fissures in a borehole wall in a laboratory scale experimental setup mimicking LWD conditions. The influence of various factors of the LWD environment on PW Doppler measurements and the limiting conditions when applied to existing LWD tools for flow quantification are also discussed. A method for estimating the fissure geometry using the PW Doppler signal is also described and compared with conventional ultrasonic pulse-echo imaging used in LWD tools.

2. Methodology

The major parameters influencing ultrasonic Doppler measurements in a LWD scenario can be narrowed down to: the geometrical constraints of the drill-string inside a borehole, properties of drilling fluid, ultrasonic transducers and associated acquisition parameters, and the motion of the drill-string. The effect of each of these parameters on PW Doppler measurements are discussed in this section.

The borehole environment typically operates under high pressure and temperature, the effect of these parameters on Doppler measurements have not been evaluated in this study.

2.1. Experimental setup

The experimental setup consists of a flow chamber as shown in Fig. 2 which emulates the geometrical and influx flow conditions inside a typical borehole. For simplicity, water is used as the working fluid for all experiments described in this paper as the sound velocity in water is close to the sound velocities typically observed in typical water-based drilling fluids (Motz et al., 1998). Water-based drilling fluids typically contain barite or bentonite as the major dispersed constituent. We dispersed cornflour in water (1 g/l) to mimic the dispersed particles in water-based drilling fluids as the typical particle size cornflour ($\approx 60\,\mu m$) is similar to barite/bentonite (≈ 40–$100\,\mu m$; Abdou and El-Sayed Ahmed, 2011). The dispersed particles in the fluid serve as Rayleigh scatterers of ultrasound which is crucial for Doppler processing. Further, the attenuation of ultrasound in water is very low compared to that is drilling fluids (Motz et al., 1998). However, ultrasound pulse-echo is routinely employed in LWD which suggest that the amplitude of 2-way ultrasound propagation between the transducer and borehole wall is usually at acceptable levels. The effect of attenuation of drilling fluids on Doppler ultrasound is not known and is beyond the scope of this work. The authors plan to study this aspect in the future.

The water with dispersed cornflour is fed into the lower part of the flow chamber which acts as a buffer to stabilize the flow before it passes through the orifice plate into the upper part of the flow chamber. The orifice plate emulates fractures in the borehole wall. The surface on which the orifice place is mounted emulates the borehole wall. The orifice plate is 3D printed with orifices of different geometries as desired to mimic fissures in the borehole wall. Fig. 3 shows two such orifice plates used for most of the experiments described in this paper. The water flows out of the orifice in the form of a jet towards the ultrasonic probe as depicted in Fig. 2. The velocity of the water jet is controlled by adjusting the inlet flow into the flow chamber. This velocity is calculated using the flow rate equation
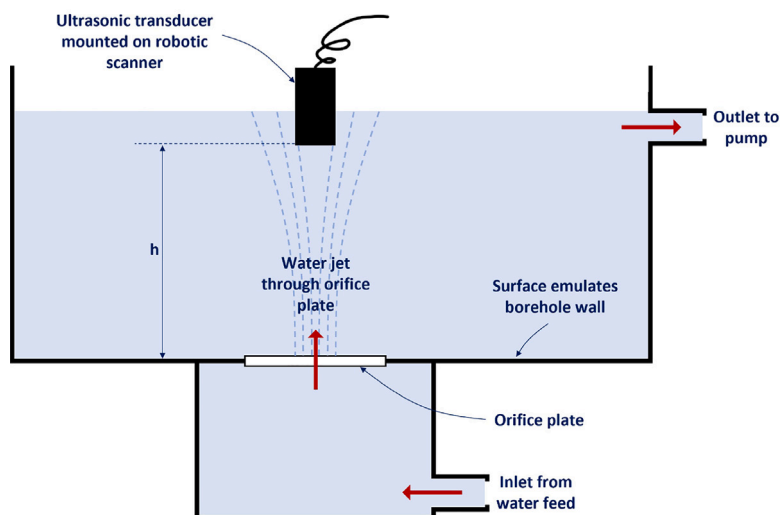
$$Q = Av, \tag{1}$$

Fig. 2. Flow chamber used in the experiments to emulate influx conditions in boreholes. (The motion of drilling fluid in axial direction of drill-string is not emulated).
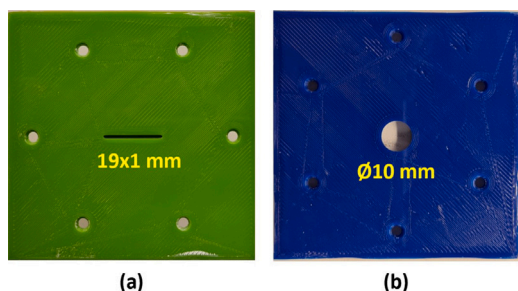

Fig. 3. Orifice plates with (a) 19 × 1 mm slot type and (b) ∅10 mm circular type orifices used with the flow chamber in Fig. 2 to emulate fractures in the borehole wall.

where Q is the flow rate through the inlet, A is the area of the orifice and v is the velocity at vena-contracta of the water jet.

The water pumped out from outlet at the top of the flow cell and is recirculated through in a closed loop. The inlet flow rate of water into the flow cell is measured using an inline ultrasonic flow meter and the flow rate is controlled by adjusting the head of the water feed tank. The feed tank is mounted on an electromagnetic stirrer to keep the dispersion of cornflour uniform throughout the experiment. Fig. 4 shows the complete experimental setup. A Verasonics Vantage 256 system (Verasonics Inc. Redmond, WA, USA) connected with a custom cannon connector PCB interface is used as the ultrasonic pulser-receiver. The acquisition and Doppler signal processing script was written in MATLAB (2019b, The Mathworks, Natick, MA, USA) and is detailed in Section 2.4.

The ultrasonic probe is mounted perpendicular to the water jet at a distance h from the orifice plate on a robotic scanner. The distance between the transducer and the orifice plate was varied between 25–50 mm in our experiments which is similar to the spacing between an ultrasonic probe and the borehole wall in typical LWD measurements (Orban et al., 2021; Maeso et al., 2018).

2.2. PW Doppler parameters

This work aims to explore an ultrasound Doppler method which can be directly applied to existing LWD tools used for imaging the borehole wall. Publications on LWD field measurements from leading drilling companies indicate the use of ultrasonic transducers in a frequency range of 100 kHz–1 MHz (Shrivastava et al., 2019; Blyth et al., 2021; Maeso et al., 2018; Longo et al., 2012; Leonard, 2016). These

publications also suggest the use of unfocused transducers, although focused transducers have also been reported in some papers. Further, the element size of the transducers, as reported in these publications, range between 1/2 to 3/4 inches in diameter.

Considering these transducer specifications, PW Doppler is well suited as it can be applied with a single element transducer and enables the measurement of radial flow velocities at multiple points along the ultrasound beam. The influence of various factors of the LWD environment on Doppler ultrasound are detailed in this section.

2.2.1. PW Doppler - fundamentals

There is a wide variety of literature on the basic principles of PW Doppler ultrasound, for example by Hoskins (2019), but a very brief overview of its fundamentals specific to the terms used in this paper are discussed here. Fig. 5 outlines the basic principles involved in PW Doppler processing. A series of ultrasonic pulses are fired into the fluid where velocity estimates are desired and the pulse-echo signals (also called as RF signals) are recorded (Fig. 5a). The time dimension in each pulse-echo signal is termed as the "fast-time" dimension which is analogous to the depth in convention pulse-echo ultrasound imaging. The firing rate or the frequency between each firing is called as the pulse repetition frequency (PRF). Several such RF signals are recorded over the "slow-time" dimension with intervals equal to PRF to form a "packet" of RF data. The number of RF signals in each packet is called as the "observation-window". The RF signals in each packet are then demodulated to obtain the in-phase quadrature (IQ) signal which contains both amplitude and phase information of the signal. The IQ signal is sampled at specific fast-time locations, producing a slow-time signal for each packet (Fig. 5b). Ths slow-time signals are then transformed into the frequency domain using Fast Fourier Transform (FFT) to obtain the PW Doppler spectra (Fig. 5c). This spectra contains information about the velocity components in the flow.

2.2.2. Velocity measurement limit

The maximum flow velocity that can be unambiguously determined using PW Doppler is given by the Nyquist limit (Hoskins, 2019) and can be expressed by

$$v_{nyq} = c \frac{\text{PRF}}{4f}, \tag{2}$$

where c is the speed of ultrasound, PRF is the pulse repetition frequency and f is the frequency of ultrasound. The PRF is the frequency of firing successive ultrasonic pulses and is limited by the 2-way transit time of ultrasound in the drilling fluid so that successive pulses do not interfere with each other. Considering the maximum spacing between
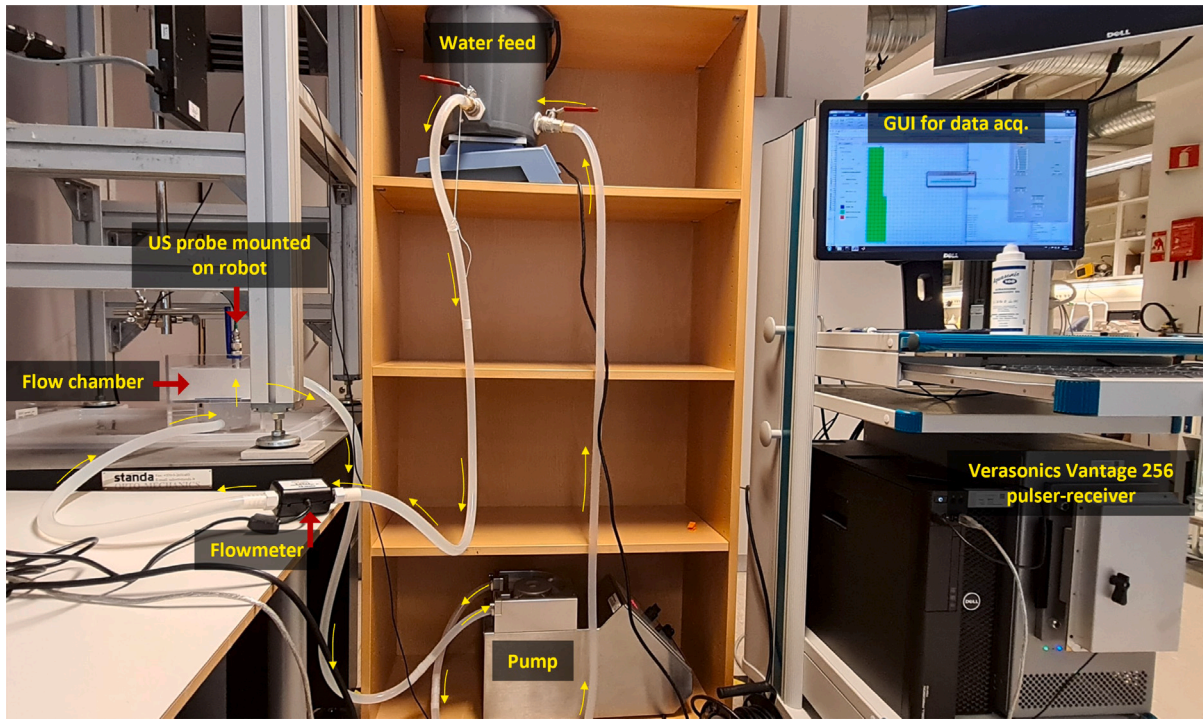
Fig. 4. Experimental setup used for PW Doppler acquisition on emulated influx conditions using the flow chamber show in Fig. 2.
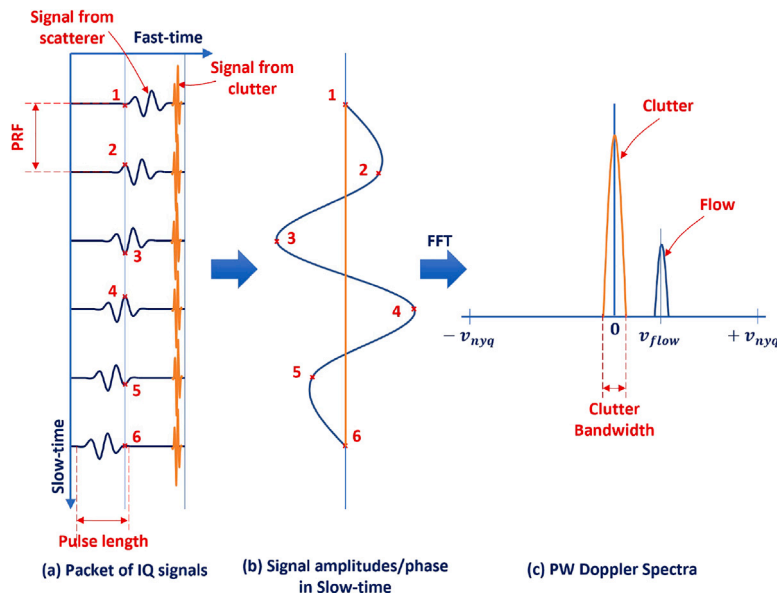

Fig. 5. Fundamentals of PW Doppler processing.

the transducer and borehole wall to be around 50 mm, the maximum PRF is theoretically limited to around 15 kHz. This will be further reduced due to any eccentricity in the BHA while drilling. Thus, in practice a PRF which is much lower than this must be used.

Furthermore, the presence of any stationary or slow-moving features within the ultrasound beam causes "clutter" in the PW Doppler spectra centered near 0 frequency (Fig. 5). Recollect that the axial flow component of the drilling fluid in the borehole (Fig. 1), which is perpendicular to the ultrasonic beam, has a typical velocity of around 2–7 m/s. Since this component is moving orthogonal to the ultrasound beam, its pulse-echo response would be similar to a stationary or slow-moving target in the fast-time dimension and thus produce clutter in the PW spectra. However, the bandwidth of this clutter would be a function of its flow

velocity in the axial direction (Yu et al., 2006) and can be calculated as

$$BW_{clutter} \approx \frac{2v_a}{W},\tag{3}$$

where v_a is the axial velocity of the drilling fluid and W is the width of the ultrasound beam.

The combined effect of these parameters defines the measurable velocity range for the influx/efflux in the radial direction of the borehole. The region between the blue and red/magenta curves in Fig. 6 shows the measurable velocity range for typical LWD ultrasonic probe frequencies and element size of 1/2 inch (12.7 mm). Low frequency transducers have a high Nyquist limit but also have a high clutter bandwidth, as seen in Fig. 6, and would not be sensitive to small
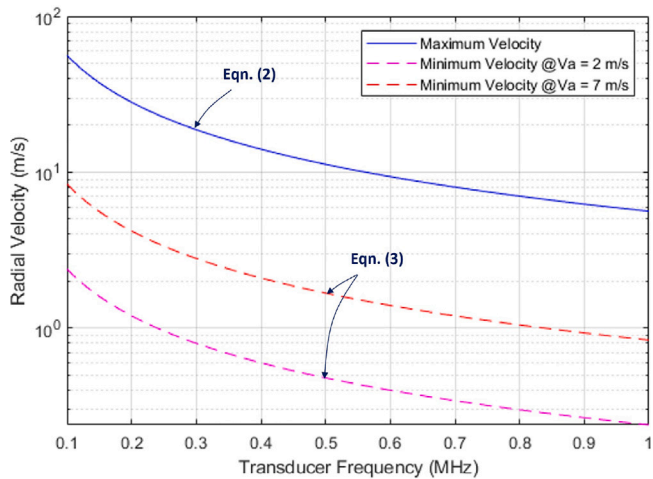
Fig. 6. Influx/efflux velocity measurement limits (upper limit: solid blue line and lower limits: dashed lines) for PW Doppler in LWD. (For interpretation of the references to color in this figure legend, the reader is referred to the web version of this article.)

Fig. 7. Nearfield length for commonly used ultrasonic transducers in LWD (solid lines) and some nearby sizes (dashed lines) for comparison. (For interpretation of the references to color in this figure legend, the reader is referred to the web version of this article.)

influx/efflux velocities. The possibility of detecting small influx/efflux velocities is crucial from an early kick detection standpoint and thereby high frequency transducers would perform better. We have used a thus selected a 1MHz transducer for the experiments discussed in this paper.

2.2.3. Nearfield of ultrasonic transducer

The nearfield of a transducer is the region very close to the transducer where the sound pressure is highly oscillatory along the ultrasound beam and therefore, for most practical purposes, it is desirable to work beyond the nearfield. The frequency and element size of the transducer influence the length of its nearfield (Krautkrämer and Krautkrämer, 1990) and this can be calculated for a transducer with a circular element using

$$N_f = \frac{D^2}{4\lambda}, \tag{4}$$

where D is the element diameter of the ultrasonic transducer and λ is the wavelength of ultrasound in the drilling fluid. It must be noted that the element diameter also influences the width of the ultrasound beam W in Eq. (3).

Fig. 7 charts out the length of nearfield for unfocused ultrasonic transducers with parameters discussed earlier. Considering that 1/2 inch (12.7 mm) and 3/4 inch (19.1 mm) transducers are most commonly used in LWD tools, we choose the smaller, 1/2 inch diameter transducer which has a nearfield of approx. 25 mm for the experiments discussed in this paper.

2.2.4. Pulse length

Velocity estimation by PW Doppler relies primarily on the back-scattered ultrasound signal from microscopic scatterers in the fluid. Rayleigh scattering is the primary mode of this back-scattered ultrasound signal and by nature is a very weak signal. The use of long pulse lengths is thus essential to obtain an adequate power of the PW Doppler signal. The pulse length is the product of the wavelength of ultrasound and the number of cycles transmitted per pulse. It directly impacts the power of the Doppler signal and spatial resolution of velocity estimates. Further, the pulse length has an inverse relationship to the bandwidth of the transmitted pulse, which influences the bandwidth of the PW Doppler spectra and in turn the accuracy of velocity estimates. Additionally, the axial resolution and variance in velocity estimates depends on the size of the sample volume used for Doppler processing, which is usually equal to the pulse length. Considering these factors,
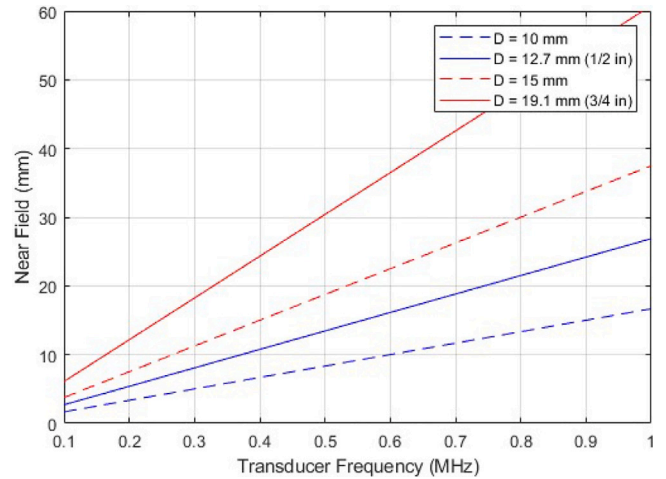
it is desired to have long pulse lengths with 8–10 λ per pulse in typical PW Doppler acquisitions. In a typical LWD scenario, the distance between the ultrasonic transducer and the borehole wall is around 25–50 mm as discussed in Section 2.1, which is equivalent to 16–32 λ for a 1 MHz ultrasonic transducer. A PW Doppler acquisition using the conventional 8–10 λ pulse, would result in the space between the transducer and borehole wall to be the equivalent of just about 2–4 sample volumes, which will yield a very low spatial resolution of velocity estimates. This paper explores the use of short pulse lengths containing 2–4 λ per pulse for obtaining high spatial resolution of velocity estimates using PW Doppler in an LWD scenario.

2.3. Motion of drill-string

The motion of a typical BHA while drilling can be broken down into its axial, circumferential and radial components as depicted in Fig. 8. The axial component is primarily the rate of penetration (ROP) and is typically around few m/hr. From an ultrasonic measurement point of view, this velocity is very low and unlikely to have any impact on acquisition parameters. The circumferential velocity is primarily due to the rotation of the BHA and is typically around 1–4 rps. Unlike conventional ultrasonic pulse-echo measurements, PW Doppler acquisitions usually require more than 50–100 signals per location for obtaining reasonably low variance in velocity estimates. In practice the ultrasound transducer would acquire these signals while the tool is rotating. Thus its acquisition rate needs to match or exceed the speed of the tool relative to the desired spatial resolution of velocity estimates in the circumferential direction. This can be calculated by

$$\text{PRF}_{min} = \frac{\omega_{\text{BHA}} \cdot R \cdot N}{\Delta x}, \tag{5}$$

where, ω_{BHA} is the angular velocity of the BHA in rad/s, R is the radius of the borehole, N is the number of ultrasound signals required for Doppler processing and Δx is the spatial resolution of velocity estimate in circumferential direction.

Radial motion of the BHA is not typically desirable, but is inevitable due to drill-string vibrations or while drilling along a deviated or horizontal direction. This causes the axis of the BHA to be eccentric relative to the borehole axis. There may also be additional vibrations of the BHA along the other directions and while there are not many published works characterizing these vibrations, Bowler et al. (2016) indicate that these were usually low frequency vibrations of around 4 Hz during their logging run. From an ultrasound Doppler standpoint, these vibrations
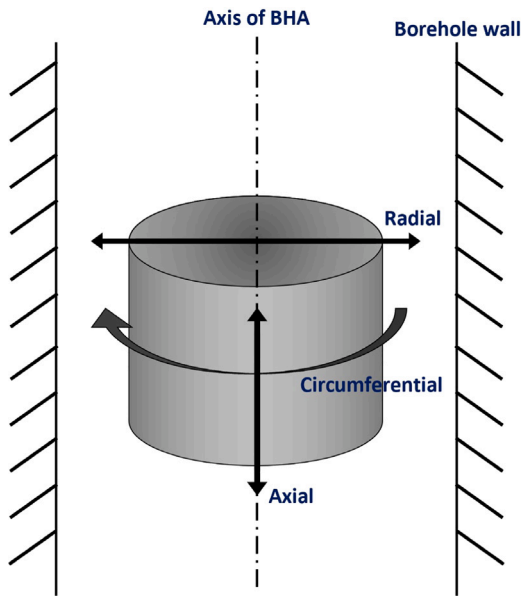
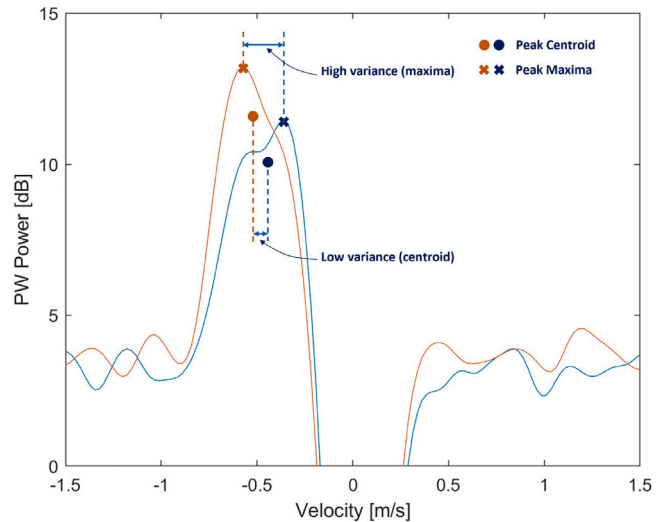**Fig. 8.** Typical motion of a BHA while drilling.

Fig. 9. Mean velocity estimate using centroid of peak in PW spectra to minimize variance between subsequent packets shown in orange and blue color. (For interpretation of the references to color in this figure legend, the reader is referred to the web version of this article.)

would cause slight broadening of the PW spectra but this would not affect the estimation of mean velocity. A PRF of 4 kHz was arbitrarily chosen, within the limits discussed earlier, for all experiments described in this paper.

2.4. Signal processing chain

RF data acquired from the Verasonics Vantage 256 system (Verasonics Inc. Redmond, WA, USA) is first reshaped into a 2D matrix with the columns representing the slow-time dimension and rows representing the fast-time dimension. The time interval between acquisitions in two adjacent columns is equal to 1/PRF. A observation-window of 200 was used for our experiments which was optimized as discussed in Section 3.1.1. A clutter filter is then applied on each of the pulse-echo acquisitions to remove the stationary and slow-moving signals caused by the initial pulse, back-wall echo and any transverse motion in the fluid column. The clutter filter used is a Kaiser windowed FIR filter of order 50 for most of the results discussed in this paper except in Section 3.1.3 which discusses the application of polynomial regression filter for reducing the observation-window. The RF signal is then demodulated to the base band to obtain the IQ signal. The PW Doppler spectra for each sample volume is then obtained by using a Hamming windowed FFT in the slow-time dimension with an 80% overlap and subsequently averaging over the fast-time dimension. The window length used for the FFT is approximately equal to the time it would take for a random scatterer in the water jet to travel a distance equal to 1 sample volume. This depends on the velocity of the water jet being evaluated. The peaks in the PW Doppler spectra are used to calculate the mean velocity of the fluid in each sample volume. Considering that we use short pulse lengths for our experiments, the PW spectra has a poor SNR and some form of dynamic threshold estimator is required for isolating the peaks in the PW spectra. An estimator utilizing the "sum of median and standard deviation" for each PW spectra was found to be effective. Further, the turbulent nature of the water jet results in a large variance in radial flow velocities of the jet at any given point in the slow-time dimension. This causes a broadening of the PW spectra and induces a high variance in the position of the peak maxima between subsequent signals at the same position. This effect is illustrated in Fig. 9 which shows the PW spectra from two subsequent packets (orange and blue) of the flow from a ⌀10 mm orifice with a velocity of 0.5 m/s. To make the peak selection unambiguous and minimize the variance in mean velocity estimates, the centroid of the PW spectra was found to be effective instead of choosing the peaks with the absolute maximum amplitude.

3. Results and discussion

3.1. Velocity estimation

The flow profile during an influx/efflux scenario is inherently complicated and would have a broad distribution of flow velocities even at a particular spatial location. Although mean the velocity at each spatial location would yield significant information for kick detection; PW Doppler has the potential to reveal the complete velocity distribution which may be leveraged for more detailed diagnostics. Fig. 10 shows the PW Doppler spectra for a mean radial flow velocity of 0.5 m/s from a ⌀10 mm orifice. The various flow velocities at each spatial location (depth) is easily evident by the spread of the PW spectra in the Y direction, and the amplitudes indicating the relative quantity of flow with specific velocity values. Further, the clutter at 0 velocity, which has been filtered out in this PW spectra, can also yield information about the flow velocity in the axial direction using Eq. (3). The PW spectra at each depth location can be analyzed individually as seen in Fig. 9 to extract the mean velocity estimates as discussed earlier.

The performance of PW Doppler on mean velocity estimates was further evaluated experimentally considering the constraints with respect to observation-window, pulse length and distance between the transducer and borehole wall.

3.1.1. Effect of observation-window on variance of mean velocity estimates

The observation-window directly influences the spatial resolution of PW Doppler when applied for LWD as explained in Section 2.3. It is therefore desirable to have small observation-windows. However, the observation-window also influences the variance of mean velocity estimates by PW Doppler and the choice of an optimal observation-window is important. Experiments using the 10 mm circular orifice (Fig. 3) and 0.3 m/s influx velocity ($\approx$ 23 ml/s) were repeated with different observation-windows and the variance in mean velocity estimates are plotted in Fig. 11. The variance seems to be leveling off by a observation-window of about 150. The observation-windows as mentioned in Fig. 11 are post clutter filtering of the RF signal and thus depending on the type of clutter filter used, the observation-window
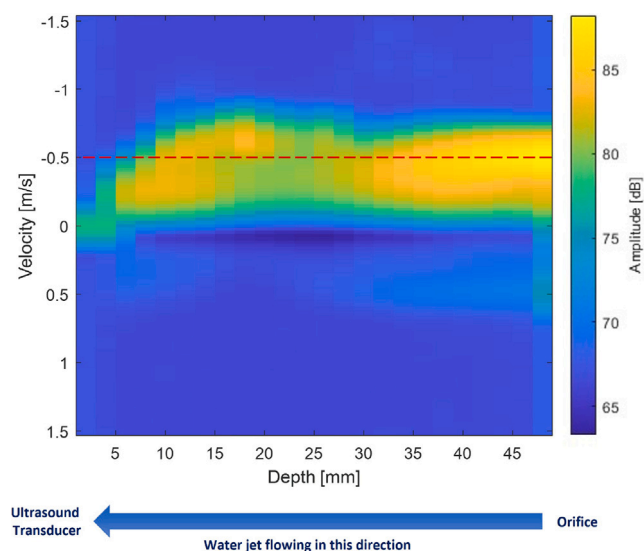
Fig. 10. PW Doppler spectra for a mean radial flow velocity of 0.5 m/s from a ⌀10 mm orifice. The dashed red line indicates the flow-meter reading for reference. (For interpretation of the references to color in this figure legend, the reader is referred to the web version of this article.)
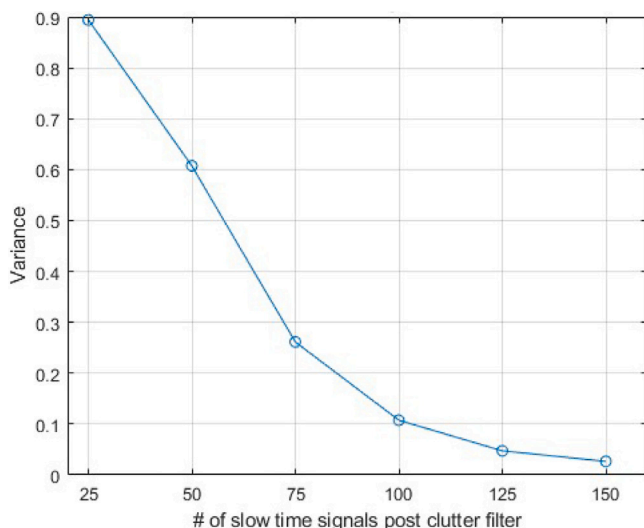

Fig. 11. Decrease in the variance of mean velocity estimates as the number of slow-time signals is increased.

should be accordingly increased while acquisition. For our experiments, an FIR filter of order 50 was found to be the most optimal, so the observation-window must be increased by 50. A observation-window of 200, including the initialization of clutter filter, was used for all experiments discussed further. Section 3.1.3 discusses a method to reduce the observation-window without compromising the variance in mean velocity estimates.

3.1.2. Effect of pulse-length on mean velocity estimates

As discussed earlier in Section 2.2.4, the constraint due to the distance between the transducer and borehole wall require the use of short pulse-length. A 2D scan was done over the ⌀10 mm orifice plate (see Fig. 3) for a radial flow velocity of 0.5 m/s and pulse-lengths equal to 2 λ and 4 λ. PW Doppler signals were acquired at 40 different points over the orifice and mean velocity estimates were calculated for each sample volume to obtain a mean velocity profile along the ultrasound beam axis. Fig. 12 shows box plots for mean velocity estimates at

each sample volume (depth) over the 40 PW Doppler signals for pulse-lengths equal to 2 λ and 4 λ. As expected, the standard deviation σ in estimates is significantly higher for 2 λ at 0.2 m/s compared to 0.05 m/s for 4 λ. The number of outliers is also significantly higher at 47 for 2 λ compared to 12 for 4 λ.

It was also attempted to acquire signals with 1 λ pulse-length, but the signal quality was too poor for Doppler processing. Acquiring signals with 2 λ was also challenging albeit possible, however it is the authors' view that it would be practically difficult to implement under field conditions. Acquisitions with 4 λ were significantly stable and easy to obtain repeatedly. For water-based drilling fluids, this would translate to a sample volume of about 6 mm, and would be the most practical choice for field conditions.

Experiments were repeated to find the lowest detectable radial flow velocity. Although there is no axial flow component in our experiments, the water jet naturally spreads out as it exits the orifice and causes some turbulence in the water chamber. This results in a broadening of the clutter signal as discussed earlier in Section 2.2.2 and the bandwidth of the clutter filter needs to be sufficiently large to accommodate it. Considering this effect, radial flow velocities from the water influx of up to 0.2 m/s (15 ml/s from ⌀10 mm orifice) were easily measurable as shown in Fig. 13.

Fundamentally there is no upper limit on the velocity measurement up to the Nyquist limit as discussed in Section 2.2.2. This translates to a limit of 5.6 m/s for a 1 MHz transducer at 15 kHz. It was however not possible to experimentally validate this for LWD using our experimental setup as the water column becomes too unstable to manage when the velocity exceeds 0.5 m/s.

3.1.3. Polynomial regression filter for reducing observation-window

The results in Section 3.1.1 suggest the use of a observation-window >150 for applying Doppler ultrasound in LWD. For a typical $6\frac{3}{4}$ inch tool moving at about 3 rps, using Eq. (5), this translates to a spatial resolution of about 16 mm for 150 signals at the maximum PRF limit of 15 kHz. This may be sufficient as a go/no-go detection for influx/efflux, but is not sufficient when high resolution measurements are desired. It is possible to reduce the tool speed to for making high resolution scans, but it is desirable if this can be avoided.

The use of FIR filters for clutter suppression is very common due to its stability, linearity and time invariant properties. These types of filters however require samples equal to the filter order for initialization, which consequentially increases the observation-window. Polynomial regression filters are known to be used in color flow imaging where there is a similar requirement of small observation-windows for high frame rate imaging (Leonov et al., 2019; Bjaerum et al., 2002). Polynomial regression filters have a steep frequency response and do not require additional samples for initialization, they are however not time invariant which makes it difficult to tune the filter to achieve a constant frequency response.

A Savitzky–Golay polynomial filter using the inbuilt MATLAB function "sgolayfilt" was implemented on the Doppler recordings with 4λ pulse-length discussed in Section 2.2.4. A filter order of 10 with a 'framelength' equal to 2 sample volumes and a order 10 kaiser-windowed weighting vector was found to be performing optimally for our recordings. The mean velocity estimates and their σ for different observation-windows are compared for a conventional kaiser-windowed FIR filter of order 50 (Fig. 14) and the Savitzky–Golay polynomial filter (Fig. 15).

The performance of FIR filter deteriorates, as evidenced by the σ, with a reduction in observation-window. The FIR filter order reduces the observation-window used for Doppler processing by 50 as discussed earlier and thus it was not possible to reduce the observation-window beyond 100. This considers that at least about 32 signals is the window length for Doppler processing as discussed in Section 2.4. Comparing this to the Savitzky–Golay polynomial filter, a minor improvement in σ is observed for all observation-windows. Further, it was possible to reduce the observation-window up to 50, since no signals are lost in the initialization of the filter, without significant loss in measurement accuracy.
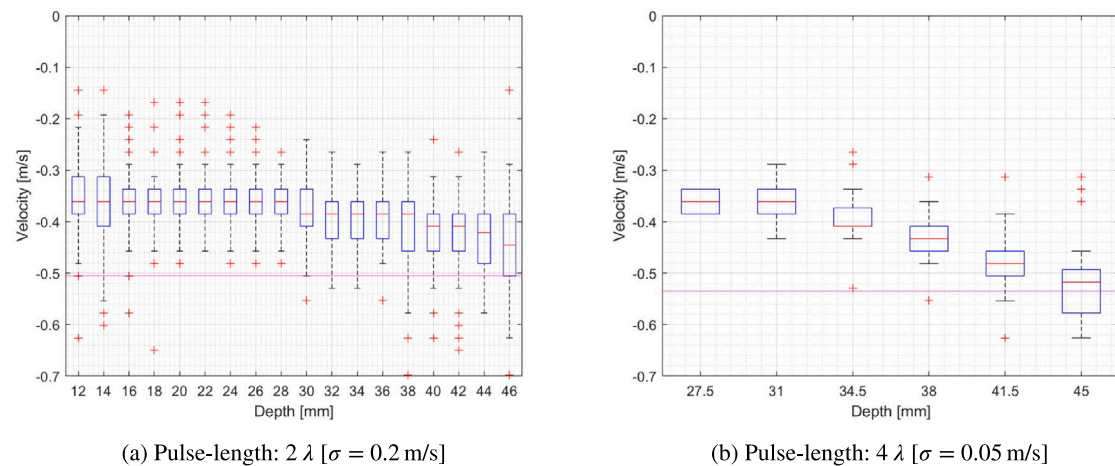
(a) Pulse-length: $2\,\lambda\ [\sigma = 0.2\,\mathrm{m/s}]$ (b) Pulse-length: $4\,\lambda\ [\sigma = 0.05\,\mathrm{m/s}]$

Fig. 12. Mean velocity estimates of 0.5 m/s influx from ∅10 mm orifice. Magenta line indicates flow-meter reading for comparison. (For interpretation of the references to color in this figure legend, the reader is referred to the web version of this article.)
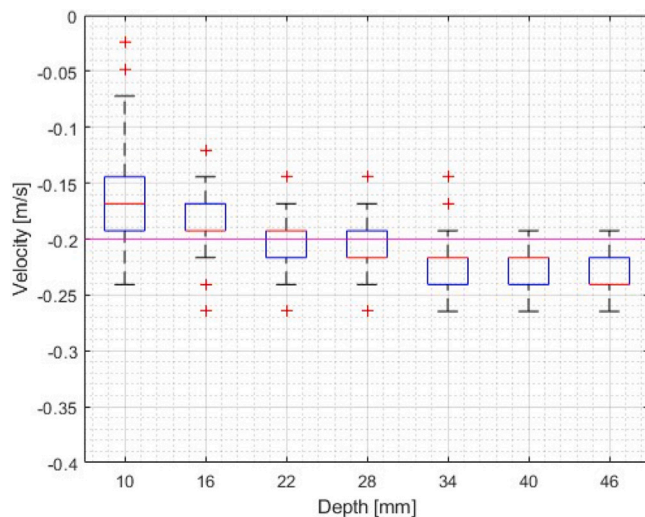

Fig. 13. Mean radial velocity profile of influx at 0.2 m/s from ∅10 mm orifice using a pulse-length of 4 λ. Magenta line indicates flow-meter reading for comparison. (For interpretation of the references to color in this figure legend, the reader is referred to the web version of this article.)

3.2. Fissure geometry estimation

Ultrasonic LWD tools are routinely employed for obtaining high resolution images of the borehole wall with one of the important objectives directed at detecting the presence of fissures on the surface of the borehole wall. The imaging resolution of such fissures however is typically very low even for high-resolution LWD tools (Li et al., 2019), partly because of the hardware limitations in incorporating such tools with the BHA. These ultrasonic LWD tools typically map the amplitude and travel time of the echo from the borehole wall for imaging.

The presence of fluid influx/efflux from such fissures provides the opportunity to process the ultrasound signal in another way viz. the Doppler spectra, which can potentially be also used for imaging the geometry of such fissures. With this objective, 2D scans were performed, using a robotic scanner as described in Section 2.1, on both the ∅10 orifice and 19 × 1 mm slot orifice plates with influx flow velocity of 0.5 m/s. The integral of the power of the IQ signal along the slow-time dimension at each measurement point was found to give the best SNR for geometry estimation and these are shown in Figs. 16(a) and 16(c). A high SNR of about 30 dB can be observed between the region with

influx (the orifice) and the regions away from the influx. Conventional backwall-amplitude images as used in LWD tools (Li et al., 2019) were also generated from the same orifice plates as shown in Figs. 16(b) and 16(d). The poor SNR of about 6 dB in these images is evident, and it is quite difficult to identify the orifices from these images. The backwall-amplitude maps in Figs. 16(b) and 16(d) have several artifacts surrounding the orifice and are caused due to geometrical features within the experimental setup and would not exist in a typical borehole setting.

Further, the dimensions of the orifice was estimated using a threshold of 96th percentile for the IQ signal power integral shown in Figs. 16(a) and 16(c). The estimated dimensions of the ∅10 orifice deviate by about −0.75 mm in Y direction and + 0.4 mm in the X direction. The deviations for the 19 × 1 mm slot orifice is about + 3.1 mm in Y direction and −0.2 mm in X direction. The deviations in the estimate in Y direction for the 19 × 1 mm slot orifice can be attributed to the point spread function (PSF) of the ultrasound transducer which is about 4 mm at 50 mm depth for the 1/2 inch, 1 MHz unfocused transducer used in these experiments. The effect of the PSF is to diffuse out the edges in an ultrasound image and this consequently causes an overestimation in the dimensional estimates. The deviations in the other dimensional estimates are relatively small and can be attributed to the variance in the signal amplitudes in the images.

4. Conclusion

The possibility of utilizing PW Doppler for the estimation of influx/efflux flow velocities and the geometry of the fissures have been explored using a laboratory scale setup. An attempt has been made to define a set of boundary conditions for the application PW Doppler in a LWD setting.

The use of short pulse-lengths and packet sizes than what is conventionally used in PW Doppler is explored and their effect on the variance of velocity estimates has been demonstrated. It has been possible to obtain mean velocity estimates with a standard deviation of 0.05 m/s using a pulse-length of 4 λ. It is also possible to use a shorter pulse-length of 2 λ but at the expense of an increase in the standard deviation of mean velocity estimates to 0.2 m/s. Though this may be a very high error for quantitative purposes, it can be useful as a radial flow detection mode when the tool to borehole wall spacing is too small for example during a phase of high tool eccentricity. It is also demonstrated that influx velocities up to a lower limit of 0.2 m/s (15 ml/s from ∅10 mm orifice) can be reliably estimated using PW Doppler.
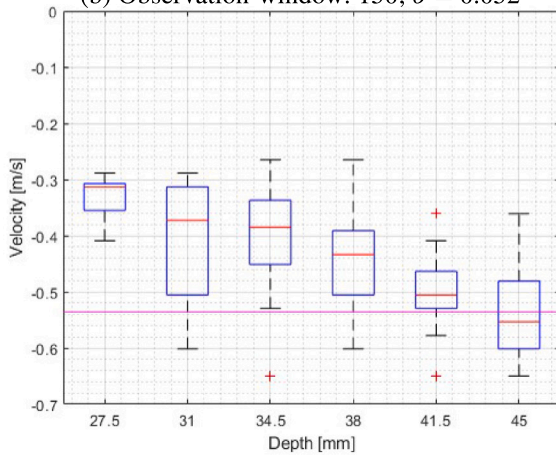
The possibility of using alternative clutter filtering methods like the Savitzky–Golay polynomial filter to reduce the observation-window of
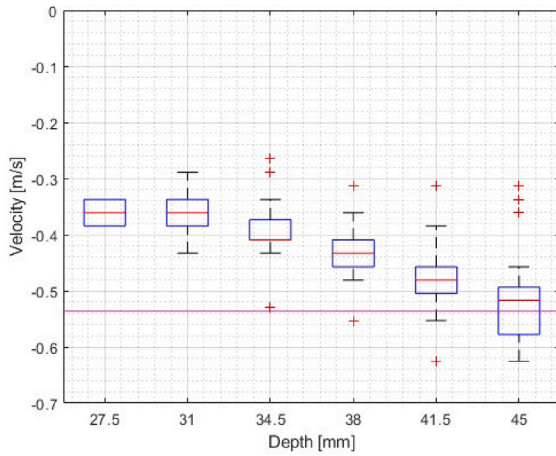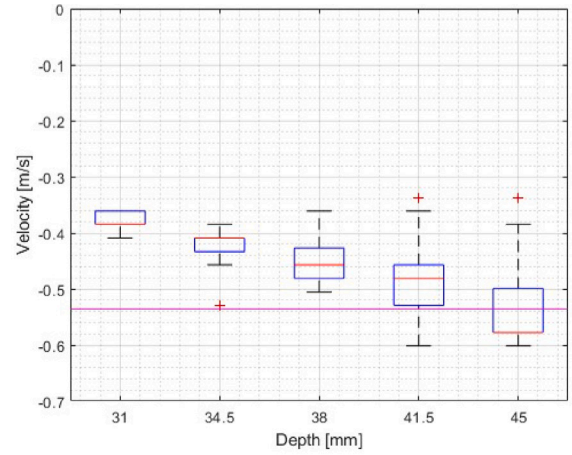
(a) Observation-window: 200; $\sigma = 0.05$

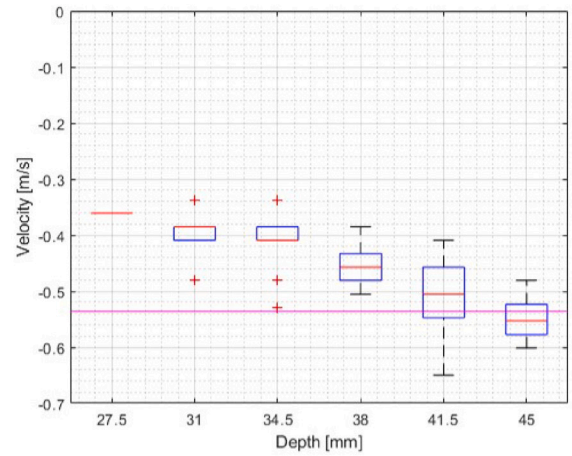(a) Observation-window: 150; $\sigma = 0.042$

(b) Observation-window: 150; $\sigma = 0.052$

(b) Observation-window: 100; $\sigma = 0.041$
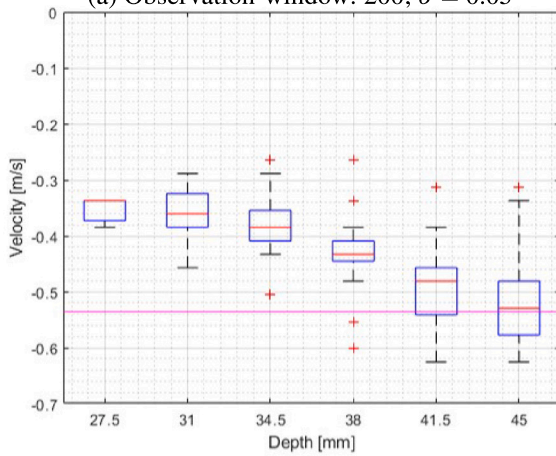
(c) Observation-window: 100; $\sigma = 0.059$
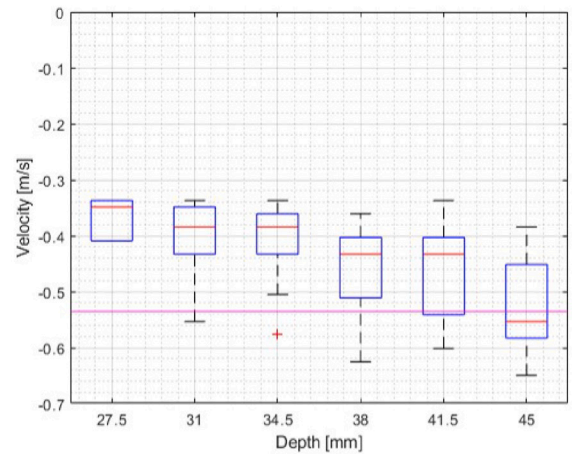
(c) Observation-window: 50; $\sigma = 0.047$

Fig. 14. Performance of kaiser-windowed FIR filter of order 50 for mean velocity estimates of 0.5 m/s influx from ⌀10 mm orifice. Magenta line indicates flow-meter reading for comparison. Indicated observation-window includes initialization size for FIR filter. (For interpretation of the references to color in this figure legend, the reader is referred to the web version of this article.)

Fig. 15. Performance of Savitzky–Golay polynomial filter of order 10 for mean velocity estimates of 0.5 m/s influx from ⌀10 mm orifice. Magenta line indicates flow-meter reading for comparison. (For interpretation of the references to color in this figure legend, the reader is referred to the web version of this article.)

PW Doppler without any adverse impact on the accuracy of mean velocity estimates is demonstrated. This is particularly useful for real-time PW Doppler acquisition while drilling at speeds of about 1–3 rps.

Lastly, the use of PW Doppler for imaging fissures and estimating their geometry with influx/efflux in boreholes is demonstrated and compared with conventional pulse-echo amplitude imaging used in
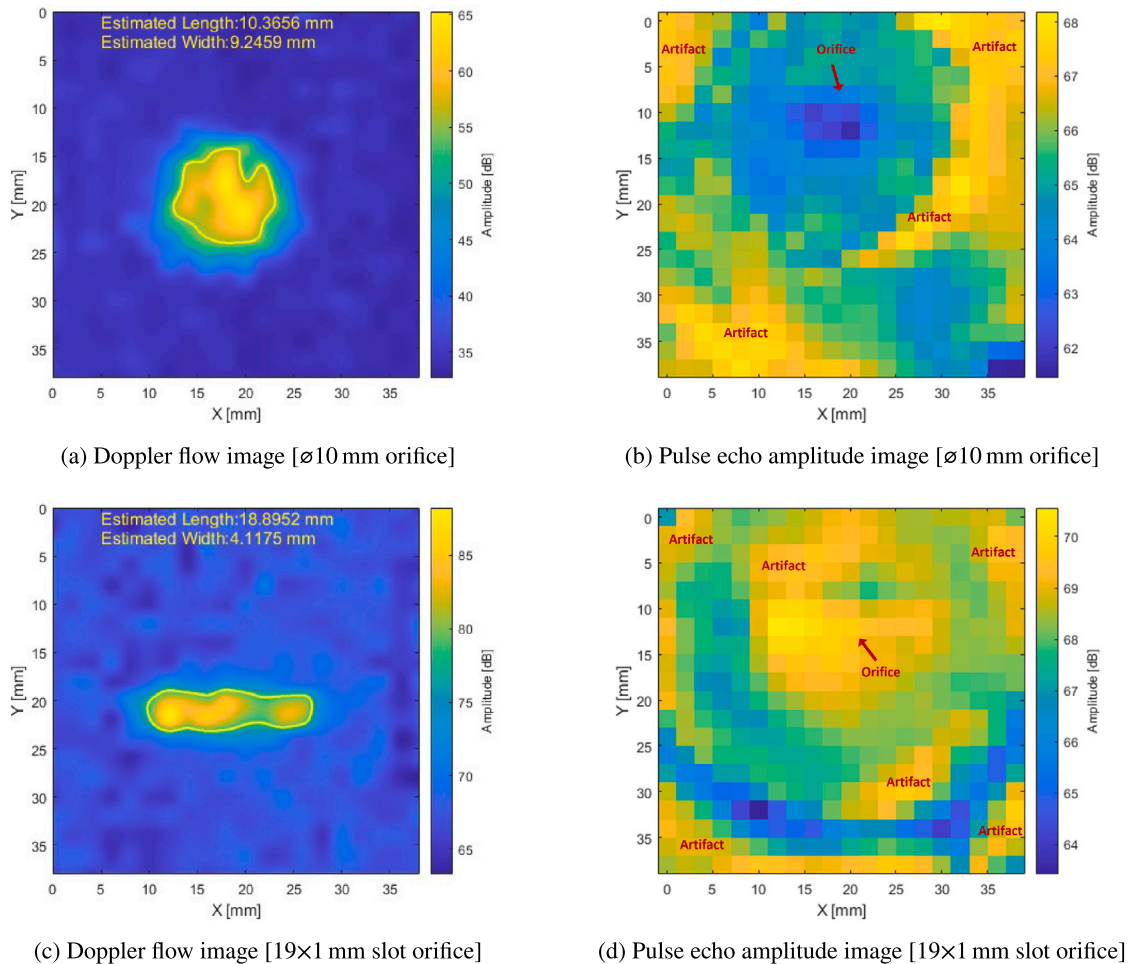
(a) Doppler flow image [⌀10 mm orifice]

(b) Pulse echo amplitude image [⌀10 mm orifice]

(c) Doppler flow image [19×1 mm slot orifice]

(d) Pulse echo amplitude image [19×1 mm slot orifice]

Fig. 16. Orifice geometry estimation using PW Doppler and pulse-echo amplitude imaging. See Fig. 3 for their true shapes.

LWD tools. PW Doppler imaging delivered a significantly higher SNR of about 30 dB compared to an SNR of about 6 dB by conventional pulse-echo amplitude imaging. Although, PW Doppler is by far the superior method compared to pulse-echo amplitude imaging, it requires an active influx/efflux from the fissure to be possible to apply. PW Doppler can thus be used as a complimentary tool in conjunction with conventional methods.

The experiments in this paper were aimed at exploring the possibility of using PW Doppler with conventional LWD tools and thus have been conducted using water as the working fluid for the sake of simplicity. Considering the promising results demonstrated in this work, further evaluation of the performance of PW Doppler using real drilling fluids of different properties should be the next step towards the deployment of this method for regular field use.

CRediT authorship contribution statement

Shivanandan Indimath: Conceptualization, Methodology, Software, Formal analysis, Investigation, Data curation, Writing – original draft, Visualization. **Stefano Fiorentini:** Software, Validation, Data curation, Writing – review & editing. **Bjarne Rosvoll Bøklepp:** Resources, Data curation, Writing – review & editing, Supervision. **Jørgen Avdal:** Software, Validation, Writing – review & editing. **Svein-Erik Måsøy:** Resources, Data curation, Writing – review & editing, Supervision, Project administration, Funding acquisition.

Declaration of competing interest

The authors declare that they have no known competing financial interests or personal relationships that could have appeared to influence the work reported in this paper.

Data availability

Data will be made available on request.

Acknowledgments

References

Abdou, M.I., El-Sayed Ahmed, H., 2011. Effect of particle size of bentonite on rheological behavior of the drilling mud. Petrol. Sci. Technol. 29 (21), 2220–2233. http://dx.doi.org/10.1080/10916461003663065, Publisher: Taylor & Francis _eprint:.

Andrew, T.A., 1942. Means for measuring flow in wells. US2277898A, URL: https://patents.google.com/patent/US2277898A/en?oq=U.S.+Patent+No.+2%2c277%2c898.

Bjaerum, S., Torp, H., Kristoffersen, K., 2002. Clutter filter design for ultrasound color flow imaging. IEEE Trans. Ultrason. Ferroelectr. Freq. Control 49 (2), 204–216. http://dx.doi.org/10.1109/58.985705, Conference Name: IEEE Transactions on Ultrasonics, Ferroelectrics, and Frequency Control.

Blyth, M., Sakiyama, N., Hori, H., Yamamoto, H., Nakajima, H., Ud Din, S.M.F., Haecker, A., Kittridge, M.G., 2021. Revealing hidden information: High-resolution logging-while-drilling slowness measurements and imaging using advanced dual ultrasonic technology. Petrophysics - SPWLA J. Form. Eval. Reserv. Descript. 62 (01), 89–108. http://dx.doi.org/10.30632/PJV62N1-2021a6.

Bowler, A., Harmer, R., Logesparan, L., Sugiura, J., Jeffryes, B., Ignova, M., 2016. Continuous high-frequency measurements of the drilling process provide new insights into drilling-system response and transitions between vibration modes. SPE Drill. Complet. 31 (02), 106–118. http://dx.doi.org/10.2118/170713-PA.

Brudy, M., Zoback, M.D., 1999. Drilling-induced tensile wall-fractures: Implications for determination of in-situ stress orientation and magnitude. Int. J. Rock Mech. Min. Sci. 36 (2), 191–215. http://dx.doi.org/10.1016/S0148-9062(98)00182-X, URL: https://www.sciencedirect.com/science/article/pii/S014890629800182X.

Chevron, Gong, B., Manuel, E., Chevron, Liu, Y., Chevron, Forand, D., Chevron, Malizia, T., Chevron, Tohidi, V., Chevron, Saldana, A., Chevron, 2021. Interpretation of lwd acoustic borehole image logs: Case studies from North American shale plays. In: SPWLA 62nd Annual Online Symposium Transactions. Society of Petrophysicists and Well Log Analysts, http://dx.doi.org/10.30632/SPWLA-2021-0085, URL: https://www.spwla.org/SPWLA/Publications/Publication_Detail.aspx?iProductCode=SPWLA-2021-0085.

Ellis, D.V., Singer, J.M., 2007. Well Logging for Earth Scientists, second ed. Springer Netherlands, http://dx.doi.org/10.1007/978-1-4020-4602-5, URL: https://www.springer.com/gp/book/9781402037382.

Ferguson, C., Klotz, J., 1954. Filtration from mud during drilling. J. Pet. Technol. 6 (02), 30–43. http://dx.doi.org/10.2118/289-G, URL: https://onepetro.org/JPT/article/6/02/30/162394/Filtration-From-Mud-During-Drilling.

Grosso, D.S., Jr., G.R.F., 1988. Method and apparatus for borehole fluid influx detection, US4733233A. URL: https://patents.google.com/patent/US4733233A/en?oq=U.S.+Patent+No.+4%2c733%2c233.

Hoskins, P.R., 2019. Principles of Doppler ultrasound. In: Diagnostic Ultrasound, third ed. 16, CRC Press, Num Pages.

Krautkrämer, J., Krautkrämer, H., 1990. Wave physics of the sound field. In: Krautkrämer, J., Krautkrämer, H. (Eds.), Ultrasonic Testing of Materials. Springer, Berlin, Heidelberg, pp. 58–92. http://dx.doi.org/10.1007/978-3-662-10680-8_5.

Leonard, Z.S., 2016. Development of a downhole ultrasonic transducer for imaging while drilling. In: 2016 IEEE International Ultrasonics Symposium. IUS, (ISSN: 1948-5727) pp. 1–4. http://dx.doi.org/10.1109/ULTSYM.2016.7728541.

Leonov, D.V., Kulberg, N.S., Fin, V.A., Podmoskovnaya, V.A., Ivanova, L.S., Shipaeva, A.S., Vladzimirskiy, A.V., Morozov, S.P., 2019. Clutter filtering for diagnostic ultrasound color flow imaging. Biomed. Eng. 53 (3), 217–221. http://dx.doi.org/10.1007/s10527-019-09912-1.

Li, P., Lee, J., Taher, A., Coates, R., Marlow, R., 2019. High-resolution ultrasonic borehole imaging enhances reservoir evaluation in oil-based muds. http://dx.doi.org/10.2118/196126-MS, OnePetro, URL: https://onepetro.org/SPEATCE/proceedings/19ATCE/2-19ATCE/D022S082R002/217774.

Longo, J., Hupp, D., Blyth, M., Alford, J., 2012. Logging-while-drilling cement evaluation: A case study from the North Slope, Alaska. http://dx.doi.org/10.2118/159819-MS, OnePetro, URL: https://onepetro.org/SPEATCE/proceedings/12ATCE/All-12ATCE/SPE-159819-MS/156344.

Maeso, C., Legendre, E., Hori, H., Auchere, J.-C., Abellan, A., Dua, R., Khan, S., Horstmann, M., 2018. Field test results of a new high-resolution, dual-physics, logging-while-drilling imaging tool in oil-base mud. OnePetro, URL: https://onepetro.org/SPWLAALS/proceedings/SPWLA18/4-SPWLA18/D043S007R001/28866.

Monnier, T., Guillermin, R., 2003. Doppler acoustic velocimetry of fluid flow from borehole fractures. p. 4.

Motz, E., Canny, D., Evans, E., 1998. Ultrasonic velocity and attenuation measurements in high density drilling muds. OnePetro, URL: https://onepetro.org/SPWLAALS/proceedings/SPWLA-1998/All-SPWLA-1998/SPWLA-1998-F/19701.

Murphy, R.D., Coope, D.F., 1985. Borehole influx detector and method, US4492865A. URL: https://patents.google.com/patent/US4492865A/en?oq=U.S.+Patent+No.+4%2c492%2c865.

Nayeem, A.A., Venkatesan, R., Khan, F., 2016. Monitoring of down-hole parameters for early kick detection. J. Loss Prev. Process Ind. 40, 43–54. http://dx.doi.org/10.1016/j.jlp.2015.11.025, URL: https://www.sciencedirect.com/science/article/pii/S0950423015300760.

Nyhavn, F., Bang, J., Øyangen, T., 1999. Production logging in horizontal wells by use of ultrasonics. SPE Prod. Facil. 14 (03), 161–165. http://dx.doi.org/10.2118/57415-PA.

Orban, J., Dennison, M., Jorion, B., Mayes, J., 1991. New Ultrasonic Caliper for MWD Operations. Society of Petroleum Engineers.

Orban, N., Garg, S., Shaldaev, M., Shrivastava, C., Zhang, T., Adrian, A., Cuadros, G., Sikdar, K., Thorat, A., 2021. Enhancement in real-time ultrasonic borehole imaging: Case study with LWD amplitude images from deepwater Brazil operations. OnePetro, URL: https://onepetro.org/OMCONF/proceedings/OMC21/All-OMC21/OMC-2021-036/473120.

Ravenscroft, F., Gulliver, J., Hayes, D., 1998. Ultrasonic flow measurement in horizontal wells. In: Offshore Technology Conference.

Razi, M., Morriss, S., Podio, A., 1995. Characterizing flow through a perforation using ultrasonic Doppler, 1995-April. pp. 943–953. http://dx.doi.org/10.2118/29544-ms, URL: https://www.scopus.com/inward/record.uri?eid=2-s2.0-85060678141&doi=10.2118%2f29544-ms&partnerID=40&md5=ab7188c9de46a536c82e376fdec7ef82.

Rodney, P.F., 1990. Detection of influx of fluids invading a borehole, US4980642A. URL: https://patents.google.com/patent/US4980642A/en?oq=U.S.+Patent+No.+4%2c980%2c642.

Saito, J., Niitsuma, H., 2001. Development of a Doppler acoustic imaging system for borehole wall to evaluate fluid flow distribution around subsurface fractures. Japan. J. Appl. Phys. 40 (Part 1, No. 5B), 3558–3561. http://dx.doi.org/10.1143/JJAP.40.3558, URL: https://iopscience.iop.org/article/10.1143/JJAP.40.3558.

Shrivastava, C., Maeso, C., Wibowo, V., Amir, I., Auchere, J.-C., Maggs, D., A, A., 2019. Multi-measurement logging-while-drilling imager: New enabler for wide-scale comprehensive geosciences applications in oil-base mud. http://dx.doi.org/10.2118/197402-MS, OnePetro, URL: https://onepetro.org/SPEADIP/proceedings/19ADIP/2-19ADIP/D021S034R004/216984.

Taherian, R., Garcia-Osuna, F., 2016. Apparatus and method for kick detection using acoustic sensors, US9494033B2. URL: https://patents.google.com/patent/US9494033B2/en?oq=U.S.+Patent+No.+9%2c494%2c033.+.

Wu, P.T., 2008. Kick warning system using high frequency fluid mode in a borehole, US7334651B2. URL: https://patents.google.com/patent/US7334651B2/en?oq=U.S.+Patent+No.+7%2c334%2c651.+.

Yu, A.C.H., Steinman, A.H., Cobbold, R.S.C., 2006. Transit-time broadening in pulsed Doppler ultrasound: A generalized amplitude modulation model. IEEE Trans. Ultrason. Ferroelectr. Freq. Control 53 (3), 530–541. http://dx.doi.org/10.1109/tuffc.2006.1610561.